

Data-Driven simulation of inelastic materials using structured data sets, tangent space information and transition rules

K. Ciftci¹, K. Hackl^{1,*}

¹*Institute of Mechanics of Materials, Ruhr-University Bochum, D-44801 Bochum, Germany.*

Abstract

Data-driven computational mechanics replaces phenomenological constitutive functions by performing numerical simulations based on data sets of representative samples in stress-strain space. The distance of modeling values, e.g. stresses and strains in integration points of a finite element calculation, from the data set is minimized with respect to an appropriate metric, subject to equilibrium and compatibility constraints, see [1, 2, 3]. Although this method operates well for non-linear elastic problems, there are challenges dealing with history-dependent materials, since one and the same point in stress-strain space might correspond to different material behavior. In [4], this issue is treated by including local histories into the data set. However, there is still the necessity to include models for the evolution of specific internal variables. Thus, a mixed formulation is obtained consisting of a combination of classical and data-driven modeling. In the presented approach, the data set is augmented with directions in the tangent space of points in stress-strain space. Moreover, the data set is divided into subsets corresponding to different material behavior, e.g. elastic and inelastic. Based on the classification, transition rules map the modeling points to the various subsets. The approach and its numerical performance will be demonstrated by applying it to models of non-linear elasticity and elasto-plasticity with isotropic hardening.

Keywords: data-driven computing, tangent space information, transition rules, inelasticity, data science

1. Introduction

The distance-minimizing data-driven computational method, introduced by Kirchdoerfer and Ortiz [1], incorporates experimental material data into numerical calculations of boundary-value problems, and therefore bypasses the empirical material modeling step. In particular, the optimization problem consists of calculating the closest point in the material data set consistent with the field equations of the problem, i.e., compatibility and equilibrium equations in continuum mechanics.

*Corresponding author

Email address: Klaus.Hackl@rub.de (K. Hackl)

For a variety of elasticity problems the approach is elaborated and the associated convergence properties are well analyzed in [2, 3, 5, 6, 7]. However, problems arise when dealing with history-dependent data as present in inelastic materials, provides one uses nearest neighbor clustering only. Therefore, local histories are included into the data set in [4]. Nonetheless, it is still necessary to resort to additional models for the evolution of internal variables. Thus a mixed formulation is obtained consisting of a combination of classical and data-driven modeling.

This paper presents a new approach by augmenting the data sets with directions in the tangent space of points in stress-strain space. A similar second order data-driven scheme, formulated by [8], uses tensor voting [9] to obtain the point-wise tangent space. In contrast, the new approach includes the tangent space directly into the distance-minimization data-driven formulation, which leads to a much more concise system of equations. Furthermore, the integration of the tangent space enables interpolation in regions of sparse data sampling, whilst ensuring the internal states to cohere with the data set. An additional step to deal with inelasticity is to classify the underlying data structure into subsets corresponding to different material behavior. Based on this, transition rules will be defined to map the internal states of the system to the various subsets.

To provide a general setting, Section 2 introduces the basic definitions and derivation of the classical distance-minimizing data-driven computing method. Section 3 presents the extension to inelasticity predicated on the extension of the data sets by tangent space information and the classification of the data into subsets corresponding to different material behavior. Additionally tangential transition rules are defined to map the modeling points to the various data subsets. Section 4 demonstrates the performance of the suggested method via numerical examples employing non-linear elasticity and elasto-plasticity with isotropic hardening. At the end, Section 5 summarizes the results and gives recommendations concerning future research topics.

2. Data-driven computing paradigm

In the following the data-driven computing paradigm will be summarized for the readers convenience based on the definitions and formulations in [1, 4]. Let $\Omega \subset \mathbb{R}^d$ with $d \in \mathbb{N}$ be a discretized system encountering displacements $\mathbf{u} = \{\mathbf{u}_i \in \mathbb{R}^{n_i}\}_{i=1}^n$ subjected to applied forces $\mathbf{f} = \{\mathbf{f}_i \in \mathbb{R}^{n_i}\}_{i=1}^n$, where $n \in \mathbb{N}$ is the number of nodes and n_i the dimension at node i .

The internal state is characterized by strain and stress pairs $\mathbf{z}_e = (\boldsymbol{\varepsilon}_e, \boldsymbol{\sigma}_e) \in \mathbb{R}^{2d_e}$ with $d_e \in \mathbb{N}$ being the dimension of stress and strain at material point $e = 1, \dots, m$, where $m \in \mathbb{N}$ is the number of material points. The internal state of the system is subject to the compatibility and equilibrium condition

$$\boldsymbol{\varepsilon}_e = \mathbf{B}_e \mathbf{u}_e, \quad \forall e = 1, \dots, m, \tag{1}$$

$$\sum_{e=1}^m w_e \mathbf{B}_e^T \boldsymbol{\sigma}_e = \mathbf{f}. \tag{2}$$

In this case w_e is a positive weight and \mathbf{B}_e is a strain-displacement matrix. Defining $\mathbf{z} = \{(\boldsymbol{\varepsilon}_e, \boldsymbol{\sigma}_e)\}_{e=1}^m$, the constraints (1) and (2) define a subspace

$$\mathcal{C} := \left\{ \mathbf{z} \in \prod_{e=1}^m \mathbb{R}^{2d_e} : (1) \text{ and } (2) \right\}, \quad (3)$$

which is denoted as constraint set. Since the set is material-independent, the connectivity between $\boldsymbol{\varepsilon}_e$ and $\boldsymbol{\sigma}_e$ is still missing. Instead of using a functional relationship, the information about the material is given by means of a data set

$$\mathcal{D} := \prod_{e=1}^m \mathcal{D}_e \quad \text{with } \mathcal{D}_e := \{(\hat{\boldsymbol{\varepsilon}}_i, \hat{\boldsymbol{\sigma}}_i) \in \mathbb{R}^{2d_e}\}_{i=1}^{n_e}, \quad (4)$$

where $n_e \in \mathbb{N}$ being the number of local data points; which classically consists of experimental measurements or data achieved from small scale simulations. To define the data-driven problem the local space \mathbb{R}^{2d_e} will be metricized by means of norms

$$\|\mathbf{z}_e\|_e := \left(\frac{1}{2} \|\boldsymbol{\varepsilon}_e\|_2^2 + \frac{1}{2} \|\boldsymbol{\sigma}_e\|_2^2 \right)^{1/2}. \quad (5)$$

To avoid the dimensional dependency, the stresses are made dimensionless by the mapping $(\boldsymbol{\sigma}_e, \hat{\boldsymbol{\sigma}}_e) \rightarrow \frac{1}{E_e}(\boldsymbol{\sigma}_e, \hat{\boldsymbol{\sigma}}_e)$, with numerical scalar $E_e \in \mathbb{R}^+$, typically being of the type of an elastic stiffness, e.g., a representative Young's modulus. The corresponding local distance function

$$d_e(\mathbf{z}_e, \hat{\mathbf{z}}_e) := \|\mathbf{z}_e - \hat{\mathbf{z}}_e\|_e \quad (6)$$

with $\mathbf{z}_e, \hat{\mathbf{z}}_e \in \mathbb{R}^{2d_e}$, can be used to define a distance for $\mathbf{z}, \hat{\mathbf{z}} \in \prod_{e=1}^m \mathbb{R}^{2d_e}$ in the global space by

$$d(\mathbf{z}, \hat{\mathbf{z}}) := \sum_{e=1}^m d_e(\mathbf{z}_e, \hat{\mathbf{z}}_e). \quad (7)$$

The distance-minimizing data driven problem, introduced by [1], reads

$$\min_{\hat{\mathbf{z}} \in \mathcal{D}} \min_{\mathbf{z} \in \mathcal{C}} d(\mathbf{z}, \hat{\mathbf{z}}) = \min_{\mathbf{z} \in \mathcal{C}} \min_{\hat{\mathbf{z}} \in \mathcal{D}} d(\mathbf{z}, \hat{\mathbf{z}}), \quad (8)$$

i.e. the aim is to find the closest point consistent with the kinematics and equilibrium laws to a material data set.

The approach as well as the convergence and well-posedness have been studied on non-linear elastic material behavior (cf. [1, 3]). In the following the data-driven paradigm will be extended to inelasticity.

3. Extension to inelasticity

In the following, we will suggest an extension of the data-driven paradigm to inelastic materials. This is a non-trivial task, since the same point in stress-strain space might correspond to different material behavior. Whereas it is proposed in [4] to include local histories into the data set, we will extend the data set by the tangent space information. Note that material tangents are accessible experimentally by appropriately varying the applied loading. For this purpose, let us introduce the extended data set

$$\mathcal{D}^\Delta = \bigtimes_{e=1}^m \mathcal{D}_e^\Delta \quad \text{with } \mathcal{D}_e^\Delta := \{(\hat{\boldsymbol{\varepsilon}}_i, \hat{\boldsymbol{\sigma}}_i) + (\Delta\hat{\boldsymbol{\varepsilon}}_i, \Delta\hat{\boldsymbol{\sigma}}_i) \in \mathbb{R}^{2d_e}\}_{i=1}^{n_e}, \quad (9)$$

where $\Delta\hat{\boldsymbol{\varepsilon}}_i, \Delta\hat{\boldsymbol{\sigma}}_i \in \mathbb{R}^{d_e}$ are tangential strain and stress increments satisfying the tangential stiffness relation

$$\Delta\hat{\boldsymbol{\sigma}}_e = \mathbf{C}_e \Delta\hat{\boldsymbol{\varepsilon}}_e, \quad (10)$$

with symmetric and positive definite matrices $\mathbf{C}_e \in \mathbb{R}^{d_e \times d_e}$. The actual independent data is then given by $(\hat{\boldsymbol{\varepsilon}}_e, \hat{\boldsymbol{\sigma}}_e, \mathbf{C}_e)$, i.e. strain, stress and tangent space, whereas $\Delta\hat{\boldsymbol{\varepsilon}}_e$ is a modeling variable in the same sense as $\boldsymbol{\varepsilon}_e$ and $\boldsymbol{\sigma}_e$, denoting the position on the tangent space at the individual data point. The main idea is the evaluation of the data point $\hat{\mathbf{z}} \in \mathcal{D}$ closest to the internal material point $\mathbf{z} \in \mathcal{C}$ and additionally closest to the local tangential direction. Thus, the presented extension uses the underlying structure in order to remain as close as possible to the local data sets.

3.1. Data-driven formulation

The definition of \mathcal{D}^Δ allows to augment the local tangent spaces directly into the distance-minimization data-driven formulation. With optimal data points $\{\hat{\mathbf{z}}_e \in \mathcal{D}_e^\Delta\}_{e=1}^m$ given, e.g. from a previous iteration, the minimization problem (8) can be written as

$$\begin{aligned} \text{Minimize} \quad & \sum_{e=1}^m d_e(\mathbf{z}_e, \hat{\mathbf{z}}_e) \\ \text{s.t.} \quad & \boldsymbol{\varepsilon}_e = \mathbf{B}_e \mathbf{u}_e, \quad \sum_{e=1}^m w_e \mathbf{B}_e^T \boldsymbol{\sigma}_e = \mathbf{f} \quad \text{and} \quad \Delta\hat{\boldsymbol{\sigma}}_e = \mathbf{C}_e \Delta\hat{\boldsymbol{\varepsilon}}_e. \end{aligned} \quad (11)$$

The compatibility constraint can be enforced by expressing the material strains in terms of displacements i.e. $\mathbf{z}_e = (\mathbf{B}_e \mathbf{u}_e, \boldsymbol{\sigma}_e)$. In addition the tangential stresses are expressed in terms of tangential strains i.e. $\hat{\mathbf{z}}_e = (\hat{\boldsymbol{\varepsilon}}_e, \hat{\boldsymbol{\sigma}}_e) + (\Delta\hat{\boldsymbol{\varepsilon}}_e, \mathbf{C}_e \Delta\hat{\boldsymbol{\varepsilon}}_e)$ ensuring the tangential stiffness relation. The equilibrium constraint can be enforced by means of Lagrange multipliers $\boldsymbol{\eta}$, leading to a Lagrangian of the form

$$\mathcal{L} = \sum_{e=1}^m d_e(\mathbf{z}_e, \hat{\mathbf{z}}_e) - \left(\sum_{e=1}^m w_e \mathbf{B}_e^T \boldsymbol{\sigma}_e - \mathbf{f} \right) \boldsymbol{\eta}. \quad (12)$$

The necessary stationary conditions of \mathcal{L} are given by

$$\delta \mathbf{u}_e : \mathbf{B}_e^T (\mathbf{B}_e \mathbf{u}_e - \hat{\boldsymbol{\varepsilon}}_e - \Delta \hat{\boldsymbol{\varepsilon}}_e) = \mathbf{0}, \quad (13)$$

$$\delta \boldsymbol{\sigma}_e : (\boldsymbol{\sigma}_e - \hat{\boldsymbol{\sigma}}_e - \mathbf{C}_e \Delta \hat{\boldsymbol{\varepsilon}}_e) = w_e \mathbf{B}_e \boldsymbol{\eta}_e, \quad (14)$$

$$\delta_{\Delta \hat{\boldsymbol{\varepsilon}}_e} : (\mathbf{B}_e \mathbf{u}_e - \hat{\boldsymbol{\varepsilon}}_e - \Delta \hat{\boldsymbol{\varepsilon}}_e) + \mathbf{C}_e (\boldsymbol{\sigma}_e - \hat{\boldsymbol{\sigma}}_e - \mathbf{C}_e \Delta \hat{\boldsymbol{\varepsilon}}_e) = \mathbf{0}, \quad (15)$$

$$\delta \boldsymbol{\eta} : \sum_{e=1}^m w_e \mathbf{B}_e^T \boldsymbol{\sigma}_e = \mathbf{f}. \quad (16)$$

Multiplying equation (14) by matrix \mathbf{C}_e and using (15) gives

$$(\mathbf{B}_e \mathbf{u}_e - \hat{\boldsymbol{\varepsilon}}_e - \Delta \hat{\boldsymbol{\varepsilon}}_e) + w_e \mathbf{C}_e \mathbf{B}_e \boldsymbol{\eta}_e = \mathbf{0}. \quad (17)$$

In addition, multiplying (17) by \mathbf{B}_e^T , using equation (13) and summing up over all material points $e = 1, \dots, m$ leads to

$$\left(\sum_{e=1}^m w_e \mathbf{B}_e^T \mathbf{C}_e \mathbf{B}_e \right) \boldsymbol{\eta} = \mathbf{0}, \quad (18)$$

which implies $\boldsymbol{\eta} = \mathbf{0}$. Consequently, equation (14) and (17) give an interpretation for the tangential increments

$$\Delta \hat{\boldsymbol{\varepsilon}}_e = \mathbf{B}_e \mathbf{u}_e - \hat{\boldsymbol{\varepsilon}}_e = \boldsymbol{\varepsilon}_e - \hat{\boldsymbol{\varepsilon}}_e, \quad (19)$$

$$\Delta \hat{\boldsymbol{\sigma}}_e = \mathbf{C}_e \Delta \hat{\boldsymbol{\varepsilon}}_e = \boldsymbol{\sigma}_e - \hat{\boldsymbol{\sigma}}_e. \quad (20)$$

Moreover, using relation (20) for equation (16) and reordering results in

$$\sum_{e=1}^m w_e \mathbf{B}_e^T \mathbf{C}_e \Delta \hat{\boldsymbol{\varepsilon}}_e = \mathbf{f} - \sum_{e=1}^m w_e \mathbf{B}_e^T \hat{\boldsymbol{\sigma}}_e. \quad (21)$$

Finally substitution of (19) into (21) the corresponding Euler-Lagrange equations resulting to the following linear equation system:

$$\left(\sum_{e=1}^m w_e \mathbf{B}_e^T \mathbf{C}_e \mathbf{B}_e \right) \mathbf{u} = \mathbf{f} - \sum_{e=1}^m w_e \mathbf{B}_e^T (\hat{\boldsymbol{\sigma}}_e - \mathbf{C}_e \hat{\boldsymbol{\varepsilon}}_e). \quad (22)$$

The global state $\mathbf{z} \in \mathcal{C}$ then follows by evaluating the local the strain increment

$$\boldsymbol{\varepsilon}_e = \mathbf{B}_e \mathbf{u}_e, \quad (23)$$

$$\boldsymbol{\sigma}_e = \hat{\boldsymbol{\sigma}}_e + \mathbf{C}_e \Delta \hat{\boldsymbol{\varepsilon}}_e = \hat{\boldsymbol{\sigma}}_e + \mathbf{C}_e (\boldsymbol{\varepsilon}_e - \hat{\boldsymbol{\varepsilon}}_e), \quad (24)$$

for all material points $e = 1, \dots, m$.

It remains to determine the optimal local data points, i.e., the stress and strain pairs

$\hat{\mathbf{z}}_e = (\hat{\boldsymbol{\varepsilon}}_e, \hat{\boldsymbol{\sigma}}_e)$ in the local data sets \mathcal{D}_e^Δ that result in the closest possible satisfaction of compatibility and equilibrium. The determination of the optimal points can be done iteratively. The iterations are performed until the distance $d(\mathbf{z}, \hat{\mathbf{z}})$ is not lower than in the iteration before or when a certain tolerance is reached. Due to the usage of the tangent-space structure, only only a few or even just one iteration are required. This constitutes a considerable increase of efficiency in comparison with the original algorithm as introduced in [1]. Moreover, because $\boldsymbol{\eta} = \mathbf{0}$, only one global system of equations have to be solved instead of two in the original algorithm.

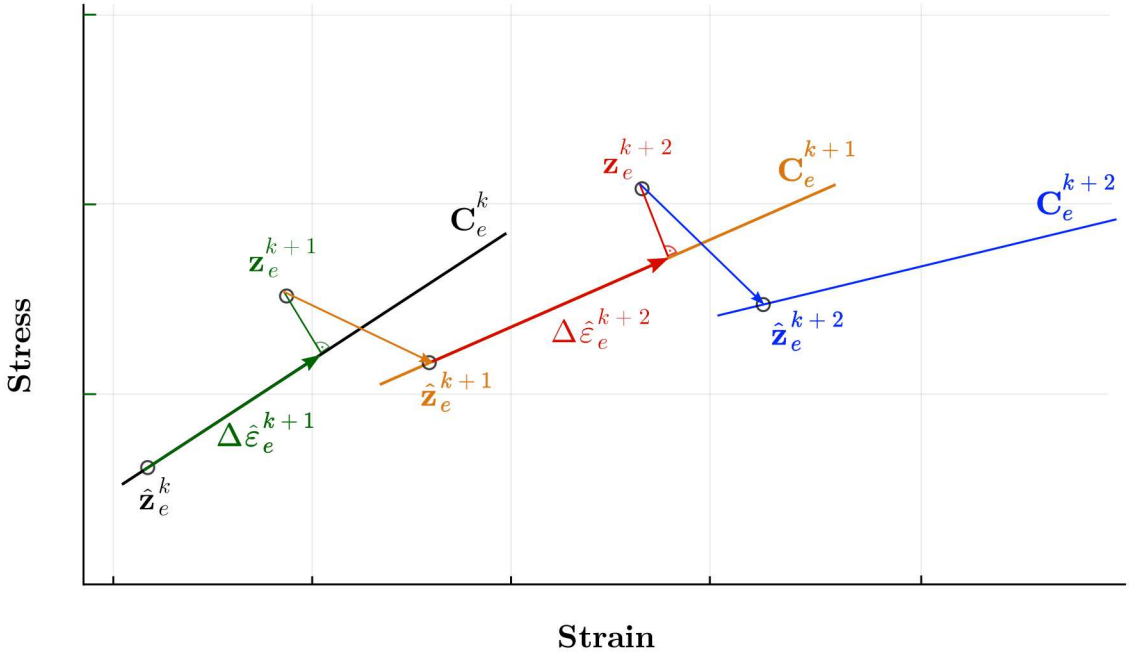


Figure 1: Visualization of data-driven method extended by tangent space. Modeling points \mathbf{z}_e^{k+1} minimize distance to the tangent space associated with data points $\hat{\mathbf{z}}_e^k$, respecting compatibility and equilibrium constraints. Data points $\hat{\mathbf{z}}_e^{k+1}$ minimize distance to modeling points \mathbf{z}_e^{k+1} .

Algorithm 1 Data-driven solver for non-linear material behavior at loading step $k + 1$

Require: strain-displacement matrices $\{\mathbf{B}_e\}_{e=1}^m$, weights $\{w_e\}_{e=1}^m$, load \mathbf{f}^{k+1} , tolerance tol

Data: data points $\{\hat{\mathbf{z}}_e^k\}_{e=1}^m$, tangent matrices $\{\mathbf{C}_e^k\}_{e=1}^m$, data sets $\{\mathcal{D}_e\}_{e=1}^m$,

function DDSOLVER($\{\mathcal{D}_e\}_{e=1}^m, \{\mathbf{C}_e^k\}_{e=1}^m, \{\hat{\mathbf{z}}_e^k\}_{e=1}^m, \mathbf{f}^{k+1}$)

while true **do**

Solve equation system:

$$\left(\sum_{e=1}^m w_e \mathbf{B}_e^T \mathbf{C}_e^k \mathbf{B}_e \right) \mathbf{u}^{k+1} = \mathbf{f}^{k+1} - \sum_{e=1}^m w_e \mathbf{B}_e^T (\hat{\boldsymbol{\sigma}}_e^k - \mathbf{C}_e^k \hat{\boldsymbol{\varepsilon}}_e^k)$$

for $e = 1 \rightarrow m$ **do**

$$\boldsymbol{\varepsilon}_e^{k+1} = \mathbf{B}_e \mathbf{u}^{k+1},$$

$$\boldsymbol{\sigma}_e^{k+1} = \hat{\boldsymbol{\sigma}}_e^k + \mathbf{C}_e^k (\boldsymbol{\varepsilon}_e^{k+1} - \hat{\boldsymbol{\varepsilon}}_e^k)$$

end for

for $e = 1 \rightarrow m$ **do**

$$\min\{d_e(\mathbf{z}_e^{k+1}, \hat{\mathbf{z}}_e) \mid \hat{\mathbf{z}}_e \in \mathcal{D}_e\}$$

end for

if $d(\mathbf{z}^{k+1}, \hat{\mathbf{z}}) \leq \text{tol}$ **then**

break

else

$$\{\hat{\mathbf{z}}_e^k\}_{e=1}^m \leftarrow \{\hat{\mathbf{z}}_e\}_{e=1}^m$$

end if

end while

return $\{\mathbf{z}_e^{k+1}\}_{e=1}^m$

end function

Given data points $\{\hat{\mathbf{z}}_e^k\}_{e=1}^m$ and tangent matrices $\{\mathbf{C}_e^k\}_{e=1}^m$ at time t^k and load \mathbf{f}^{k+1} at time

t^{k+1} , the modeling points $\{\mathbf{z}_e^{k+1}\}_{e=1}^m$ and data points $\{\hat{\mathbf{z}}_e^{k+1}\}_{e=1}^m$ are calculated. Fig. 1 gives a visualization of a single algorithmic loading step. The data-driven solver for non-linear material behavior using fixed-point iteration is summarized in Algorithm 1.

3.2. Tangential transition rules

To simulate inelastic material behavior, the main task is to capture history dependence. This is achieved by associating different tangent spaces to data points with different history. Assuming an underlying data structure, as proposed in [8], the local material data sets \mathcal{D}_e^Δ are classified into subsets corresponding to different material behavior, e.g. elastic and inelastic:

$$\mathcal{D}_e^\Delta = \bigcup_p \mathcal{D}_e^{\Delta,p} \quad \text{with } p = \{\text{elastic, inelastic}\}. \quad (25)$$

Thus, data points with close or even the same strain and stress values may possess vastly different tangent spaces; in the elastic case essentially determined by the elastic stiffness and in the plastic case by the hardening modulus. It should be emphasized that it is easily possible to distinguish experimentally between elastic and plastic material behavior. Based on the classification, transition rules map the modeling points to the various subsets.

In the following, a transition mapping is derived for the case of elasto-plasticity with isotropic hardening. The kinetics of elasto-plasticity is governed by a yield condition of the form

$$\sigma_{\text{com}}(\boldsymbol{\sigma}) \leq \sigma_y, \quad (26)$$

where $\sigma_{\text{com}}(\boldsymbol{\sigma})$ is a comparison stress dependent on the current stress state, e.g. $\sigma_{\text{com}}(\boldsymbol{\sigma}) = \sqrt{3/2} \|\text{dev} \boldsymbol{\sigma}\|$ in the case of von Mises (J_2) plasticity, and σ_y denotes the yield stress, a material property depending on the loading history in the case of isotropic hardening. For $\sigma_{\text{com}}(\boldsymbol{\sigma}) < \sigma_y$, we have elastic behavior, for $\sigma_{\text{com}}(\boldsymbol{\sigma}) = \sigma_y$ plastic behavior.

Given values of modeling points $\{\mathbf{z}_e^{k+1}\}_{e=1}^m$ using the data-driven algorithm 1, the transition mapping for material state $e = 1, \dots, m$ at loading step $k + 1$ can be formulated as:

- (i) assign local data set $\tilde{\mathcal{D}}_e$ by

$$\tilde{\mathcal{D}}_e = \mathcal{D}_e^{\Delta,p} \quad \text{with } p \equiv \begin{cases} \text{elastic,} & \text{if } \sigma_{\text{com}}(\boldsymbol{\sigma}_e^{k+1}) < \sigma_{y,e} \\ \text{inelastic,} & \text{otherwise.} \end{cases} \quad (27)$$

- (ii) if $p \equiv \text{inelastic}$, set new yield stress at $\sigma_{y,e} := \sigma_{\text{com}}(\boldsymbol{\sigma}_e^{k+1})$;

- (iii) find closest data point $\hat{\mathbf{z}}_e^{k+1}$ in data set $\tilde{\mathcal{D}}_e$ to modeling points \mathbf{z}_e^{k+1} with

$$\min\{d_e(\mathbf{z}_e^{k+1}, \hat{\mathbf{z}}_e^{k+1}) \mid \hat{\mathbf{z}}_e^{k+1} \in \tilde{\mathcal{D}}_e\}. \quad (28)$$

While step (i) maps the modeling points to the corresponding data sets, steps (ii) and (iii) define a new yield limit and find the closest data point inside these sets for the next loading

increment. These formulations give rise to corresponding representational scheme in the context of data-driven inelasticity, which are summarized in Algorithm 2.

Algorithm 2 Data-driven transition rules for inelasticity at loading step $k + 1$

Require: load \mathbf{f}^{k+1} , yield stresses $\{\sigma_{y,e}\}_{e=1}^m$

Data: data points $\{\hat{\mathbf{z}}_e^k\}_{e=1}^m$, tangent matrices $\{\mathbf{C}_e^k\}_{e=1}^m$, data sets $\{\tilde{\mathcal{D}}_e\}_{e=1}^m$, data subsets $\{(\mathcal{D}_e^{\Delta, \text{elastic}}, \mathcal{D}_e^{\Delta, \text{inelastic}})\}_{e=1}^m$

$$\{\mathbf{z}_e^{k+1}\}_{e=1}^m = \text{DDSOLVER}(\{\tilde{\mathcal{D}}_e\}_{e=1}^m, \{\mathbf{C}_e^k\}_{e=1}^m, \{\hat{\mathbf{z}}_e^k\}_{e=1}^m, \mathbf{f}^{k+1})$$

for $e = 1 \rightarrow m$ **do**

if $\sigma_{\text{com}}(\boldsymbol{\sigma}_e^{k+1}) < \sigma_{y,e}$ **then**

$$\tilde{\mathcal{D}}_e \equiv \mathcal{D}_e^{\Delta, \text{elastic}}$$

else

$$\tilde{\mathcal{D}}_e \equiv \mathcal{D}_e^{\Delta, \text{inelastic}}$$

$$\sigma_{y,e} = \sigma_{\text{com}}(\boldsymbol{\sigma}_e^{k+1})$$

end if

$$\min\{d_e(\mathbf{z}_e^{k+1}, \hat{\mathbf{z}}_e^{k+1}) \mid \hat{\mathbf{z}}_e^{k+1} \in \tilde{\mathcal{D}}_e\}$$

end for

4. Numerical results for a 2D problem

In this section the performance of the presented data-driven solver extended by the tangential space information will be illustrated in a typical benchmark example considering a rectangular plate with a circular hole under loading (cf. Fig. 2). The plate has the dimensions of $1 \text{ m} \times 0.2 \text{ m}$, is clamped at its left edge and subjected to a uniform vertical load at its right edge.

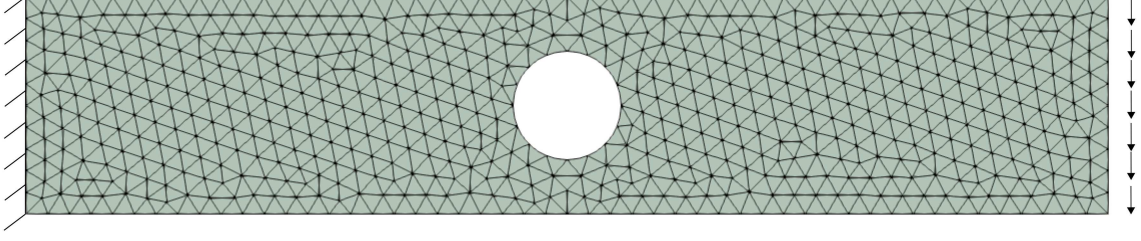


Figure 2: Discretization and boundary conditions for a rectangular plate with a circular hole under loading.

The following simulations deal with the analysis of a non-linear elastic material and an elasto-plastic von Mises material with isotropic hardening. Notice that the error between a data-driven solution \mathbf{z}^k and its corresponding reference solution $\mathbf{z}^{k,\text{ref}}$ shall be calculated by means of the root-mean-square deviation of strain and stress defined by

$$\text{RMSD}(\mathbf{z})^2 = \frac{\sum_{k=0}^T \text{Error}(\mathbf{z}^k)^2}{T}, \quad (29)$$

where $T \in \mathbb{N}$ is the number of total loading steps, $\mathbf{z}_e^k = (\boldsymbol{\varepsilon}_e^k, \boldsymbol{\sigma}_e^k)$ the local data-driven states and $\mathbf{z}_e^{k,\text{ref}} = (\boldsymbol{\varepsilon}_e^{k,\text{ref}}, \boldsymbol{\sigma}_e^{k,\text{ref}})$ the local reference states at step $k \leq T$. The error is given by

$$\text{Error}(\mathbf{z}^k)^2 = \frac{\sum_{e=1}^m w_e \|\mathbf{z}_e^k - \mathbf{z}_e^{k,\text{ref}}\|^2}{\sum_{e=1}^m w_e \|\mathbf{z}_e^{k,\text{ref}}\|^2}, \quad (30)$$

with $\|\cdot\|$ given by definition (5).

4.1. Example: non-linear elasticity

In the following, we are considering a non-linear elastic model. The material parameters of the reference solid used for the reference solution and data sets are Young's modulus $E = 100 \cdot 10^8$ Pa, Poisson's ratio $\nu = 0.3$ and elasticity matrix

$$\mathbf{C} = \frac{E}{(1+\nu)(1-2\nu)} \begin{pmatrix} 1-\nu & \nu & 0 \\ \nu & 1-\nu & 0 \\ 0 & 0 & \frac{1}{2}(1-2\nu) \end{pmatrix}. \quad (31)$$

The response is computed using a non-linear relation defined by

$$\boldsymbol{\sigma} = \lambda f(\text{tr}(\boldsymbol{\varepsilon})) \mathbf{1} + \mu \boldsymbol{\varepsilon} + \mathbf{C} \boldsymbol{\varepsilon}$$

with $f(x) := c_1 \tanh(c_2 x)$, parameters $c_1 = 0.005$, $c_2 = 0.8 \cdot 10^3$, identity matrix $\mathbf{1}$ and Lamé constants λ, μ defined by

$$\lambda = \frac{E\nu}{(1+\nu)(1-2\nu)} \quad \text{and} \quad \mu = \frac{E}{2(1+\nu)}. \quad (32)$$

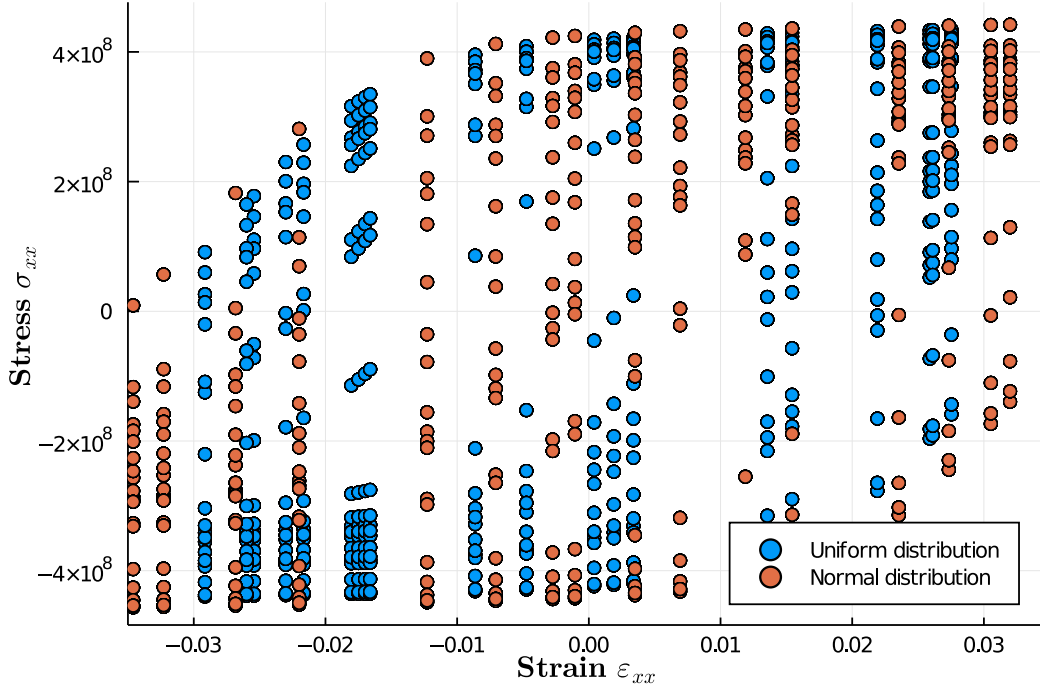


Figure 3: Projection of the data set to the ε_{xx} - σ_{xx} -plane, according to non-linear elastic material behavior within a normal and uniform distribution setting.

For the data-driven computation two different types of data distributions are investigated. The first data set is created by a zero-mean normal distribution with a standard deviation of 0.001 and the second data set is created by a uniform distribution within $[-0.03, 0.03]$ for strains in each direction. Figure 3 visualizes both distribution settings. The apparent vertical alignment of the data set is an artifact produced by the projection onto the $\varepsilon_{xx} - \sigma_{xx}$ - plane. Finally, the simulation of problem in Fig. 2 is performed by applying a load increasing from 0 to $1.8 \cdot 10^7$ Pa with 100 incremental steps using a constant normalized time step of $\Delta t = 1$. Due to the random nature of the data distribution, each simulation returns a different error. To cover a wide spectrum of the errors produced, we run 100 simulations corresponding to independent realizations of both distributions.

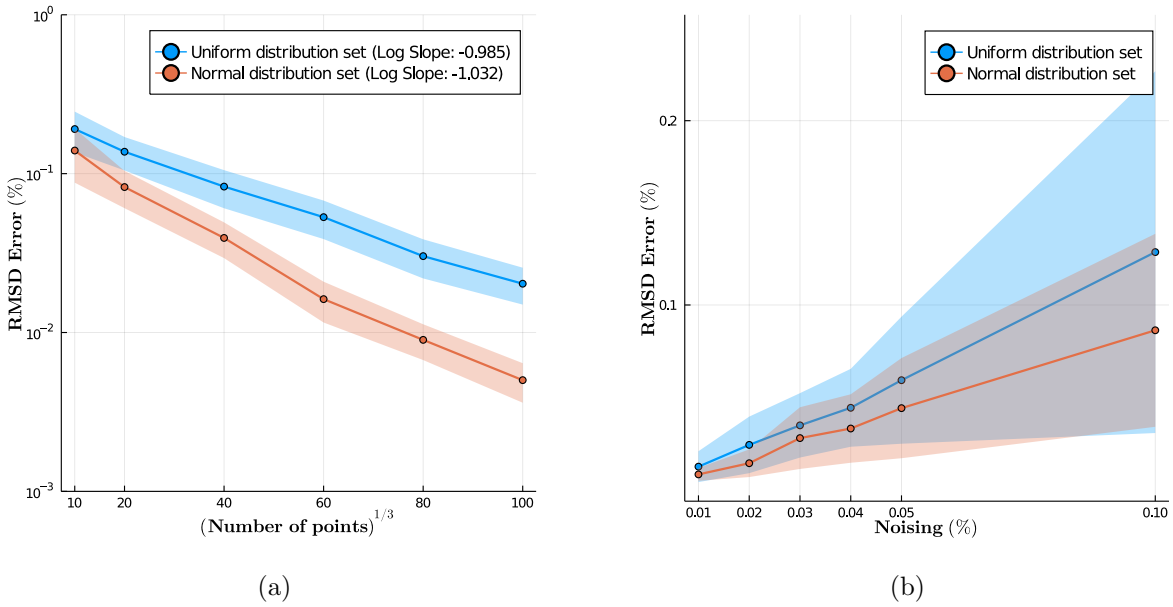


Figure 4: RMSD Error of data-driven solver for normal and uniform distributed data points. (a) Convergence with respect to data size. (b) Dependency of the error on applied noising. The shaded areas show the spread of the error arising from the different data set realizations.

The error plot in Fig. 4a shows a linear rate of convergence, which corresponds to the data-driven convergence analysis of elastic problems in [1]. Figure 4b shows the dependence of the error from noising ranging from 1% to 10% of the maximum values of strains and stresses applied to the various data sets. The shaded areas show the spread of the error arising from the different data set realizations used in the independent simulation runs. Note, that apparently data sets with normal distribution give better performance.

4.2. Example: elasto-plasticity with isotropic-hardening

This example illustrates the performance of the data-driven method extended by transition rules by considering an elasto-plastic von Mises material with isotropic hardening for the boundary value problem in Fig. 2. The material parameters of the reference solid used for the reference solution and data sets are Young's modulus $E = 200 \cdot 10^9$ Pa, Poisson's ratio $\nu = 0.3$, isotropic hardening modulus $H = E/20$, initial yield stress $\sigma_{y0} = 250 \cdot 10^6$ Pa and elasticity matrix given by (31). The response is computed in a standard manner using a J_2 -plasticity model based on an iterative predictor-corrector return mapping algorithm embedded in a Newton-Raphson global loop to restore equilibrium.

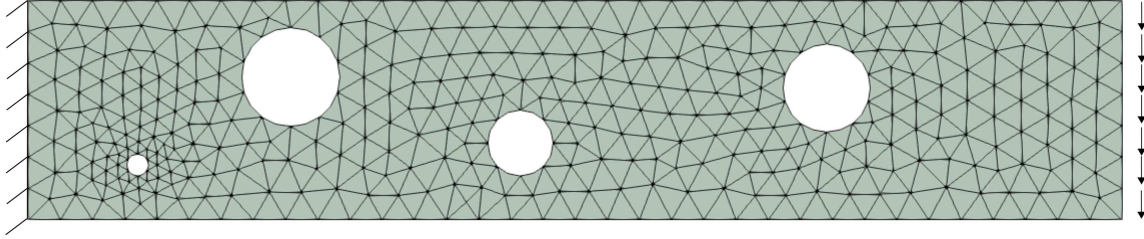
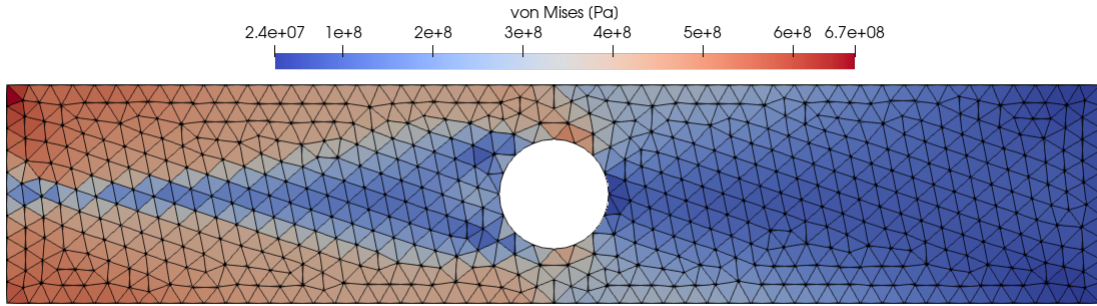
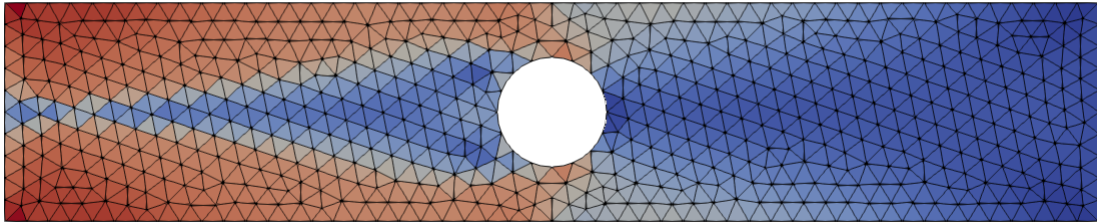


Figure 5: A virtual test of a plate with random holes to generate suitable data sets.



(a) Reference solution



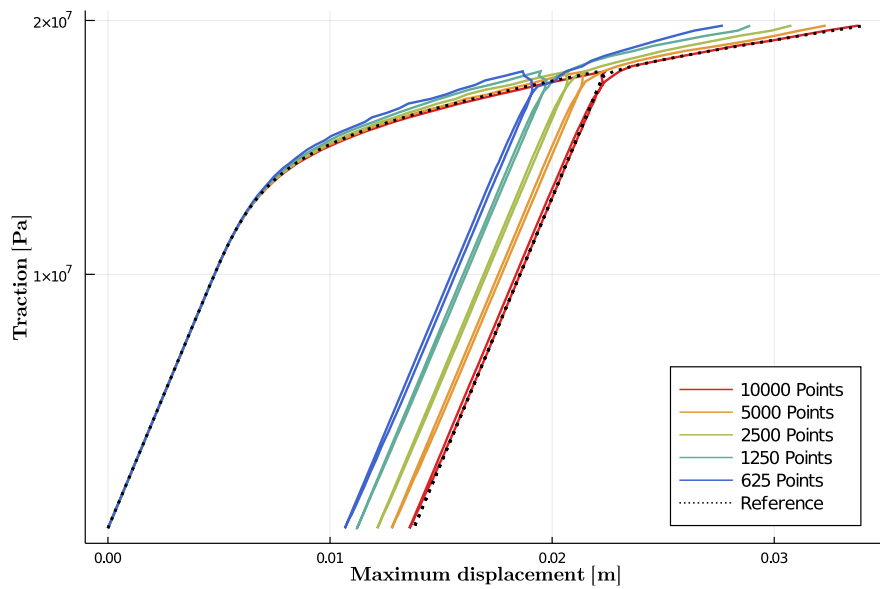
(b) Data-driven solution

Figure 6: Von Mises stress distribution at maximum loading at each Gaussian integration point using (a) J_2 -plasticity model and (b) data-driven algorithm.

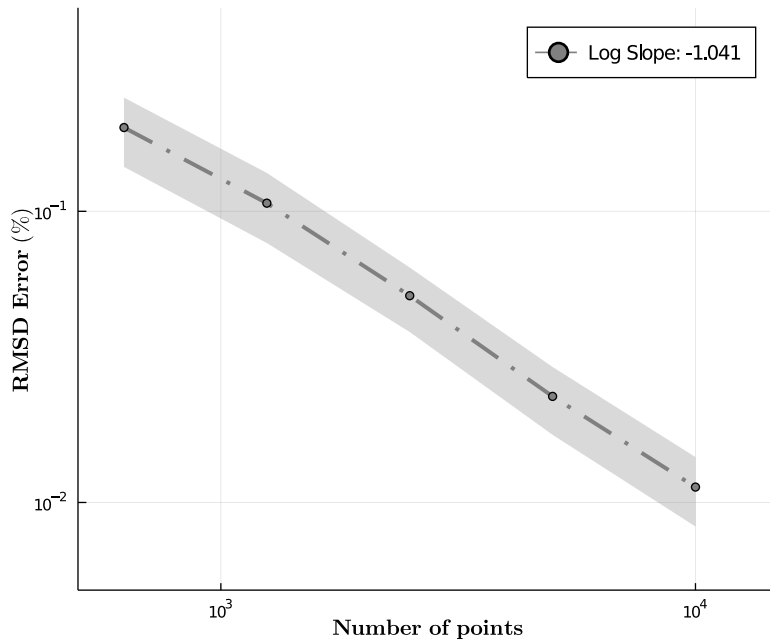
Following [4], a virtual test employing the geometry depicted in Fig. 5 is used to generate an accurate coverage of suitable local material states and loading paths of various set sizes. For the data-driven simulation, the geometry shown in Fig. 2 is used again. The applied load increases from 0 to $1.8 \cdot 10^7$ Pa, decreases to 0 and then increases again to $2 \cdot 10^7$ Pa, using a constant normalized time step of $\Delta t = 1$.

Figure 6 shows the data-driven solution at the maximum loading magnitude using a data sample containing 10^4 points. The convergence of the maximum displacement to the reference displacement based on a J_2 -plasticity model can be seen in Fig. 7a. Moreover, Fig. 7b confirms a linear convergence rate towards the reference solution by increasing the number of data points. For better representation, the convergence of the displacement is

shown for only one virtual test. However, the convergence of the error is shown for various virtual tests leading to a deviation visualized by the shaded area.



(a)



(b)

Figure 7: Convergence property of the extended data-driven method using tangential transition rules for elasto-plastic material behaviour. (a) Maximum displacement (vertical displacement of lower right vertex versus traction (resultant load of right edge) for different data resolution. (b) RMSD Error for each data resolution. The shaded area shows the deviation of the error arising from different independent virtual tests.

5. Conclusions

We present an approach extending the model-free data-driven computing method of problems in elasticity of Kirchdoerfer and Ortiz [1] to inelasticity. The original method uses nearest neighbor clustering and therefore challenges arise dealing with history-dependent data. This issue is treated in this work by extending the formulation by including point-wise tangent spaces and classifying the data structure into subsets corresponding to different material behavior. Based on the classification, transition rules are defined to map the material point to the classified data subsets, which incorporates with the idea that data points are connected by an underlying structure to each other. Additionally, minimizing the distance to local tangent spaces ensures data point connectivity and enables interpolation in regions lacking information of data.

Furthermore, the presented scheme can be easily applied to non-linear elasticity as well, noticing that the resulting system of equations of the minimization problem is reduced, leading to greater efficiency. A numerical example has been presented to demonstrate the application to data-driven inelasticity and its numerical performance.

Generally, it can be concluded that improvements in accuracy of the presented approach increase for larger data sets and it correlates with the convergence analysis of data-driven elasticity. Nevertheless, it should be mentioned that the ensurance of specific quality of the data such as good coverage of material states and loading paths constitutes a critical issue concerning the availability of real experimental data. Another issue concerns the classification of the data into subsets corresponding to material behavior. This could be done by efficient machine-learning algorithms e.g. spectral or density based clustering. These generalizations of the data-driven paradigm suggest important directions for future research, especially the usage of machine-learning methods providing further improvement and automation.

References

- [1] Trenton Kirchdoerfer and Michael Ortiz. Data-driven computational mechanics. *Computer Methods in Applied Mechanics and Engineering*, 304:81–101, 2016.
- [2] Trenton Kirchdoerfer and Michael Ortiz. Data driven computing with noisy material data sets. *Computer Methods in Applied Mechanics and Engineering*, 326:622–641, 2017.
- [3] S. Conti, S. Müller, and M. Ortiz. Data-driven problems in elasticity. *Archive for Rational Mechanics and Analysis*, 229(1):79–123, Jan 2018.
- [4] Robert Eggersmann, Trenton Kirchdoerfer, Stefanie Reese, Laurent Stainier, and Michael Ortiz. Model-free data-driven inelasticity. *Computer Methods in Applied Mechanics and Engineering*, 350:81–99, 2019.
- [5] Trenton Kirchdoerfer and Michael Ortiz. Data-driven computing in dynamics. *International Journal for Numerical Methods in Engineering*, 113(11):1697–1710, 2018.

- [6] Laurent Stainier, Adrien Leygue, and Michael Ortiz. Model-free data-driven methods in mechanics: material data identification and solvers. *Computational Mechanics*, pages 1–13, 2019.
- [7] Armin Galetzka, Dimitrios Loukrezis, and Herbert De Gersen. Data-driven solvers for strongly nonlinear material response. *ArXiv*, abs/2008.08482, 2020.
- [8] R. Eggersmann, L. Stainier, M. Ortiz, and S. Reese. Model-free data-driven computational mechanics enhanced by tensor voting. *ArXiv*, abs/2004.02503, 2020.
- [9] Philippos Mordohai and Gérard Medioni. Dimensionality estimation, manifold learning and function approximation using tensor voting. *Journal of Machine Learning Research*, 11:411–450, 01 2010.